www.MaterialsViews.com

ADVANCED FUNCTIONAL MATERIALS
www.afm-journal.de

FULL PAPER

Ultrasmall Dispersible Crystalline Nickel Oxide Nanoparticles as High-Performance Catalysts for Electrochemical Water Splitting

Ksenia Fominykh, Johann M. Feckl, Johannes Sicklinger, Markus Döblinger, Sebastian Böcklein, Jürgen Ziegler, Laurence Peter, Jiri Rathousky, Ernst-Wilhelm Scheidt, Thomas Bein, and Dina Fattakhova-Rohlfing**

Ultrasmall, crystalline, and dispersible NiO nanoparticles are prepared for the first time, and it is shown that they are promising candidates as catalysts for electrochemical water oxidation. Using a solvothermal reaction in *tert*-butanol, very small nickel oxide nanocrystals can be made with sizes tunable from 2.5 to 5 nm and a narrow particle size distribution. The crystals are perfectly dispersible in ethanol even after drying, giving stable transparent colloidal dispersions. The structure of the nanocrystals corresponds to phase-pure stoichiometric nickel(II) oxide with a partially oxidized surface exhibiting Ni(III) states. The 3.3 nm nanoparticles demonstrate a remarkably high turn-over frequency of 0.29 s^{-1} at an overpotential of $\gamma = 300$ mV for electrochemical water oxidation, outperforming even expensive rare earth iridium oxide catalysts. The unique features of these NiO nanocrystals provide great potential for the preparation of novel composite materials with applications in the field of (photo)electrochemical water splitting. The dispersed colloidal solutions may also find other applications, such as the preparation of uniform hole-conducting layers for organic solar cells.

1. Introduction

Nickel(II) oxide (NiO) is an abundant and technologically important semiconducting oxide. The main applications of nickel oxide, such as catalysis,[1] batteries,[2] supercapacitors,[3] electrochromics,[4] sensors[5] and many others can often benefit from nanostructuring and from reducing the crystal size down to the nanometer scale. Due to a greatly increased interface and drastically reduced dimensions relative to the bulk, the reported nickel oxide nanomorphologies such as nanoflowers,[6,7] porous spheres,[8] nanowires[9] or nanotubes[10] generally demonstrate superior performance in applications involving charge transfer and charge transport processes.[11] Crystalline non-agglomerated dispersible nanoparticles of NiO are attractive because colloidal nanocrystal dispersions can be used for the controlled deposition of crystalline nickel oxide at room temperature, or for the fabrication of hole transporting layers in polymer solar cells.[12] Furthermore, a reduction in the crystal size to only a few nanometers is expected to modify the electronic, optical and magnetic characteristics of the nanocrystals as well as their surface properties.

Although colloidal non-agglomerated nanocrystals can be obtained for several other metal oxides,[13] nickel oxide in this form has not been available so far. NiO can be easily prepared by a range of chemical and physical methods.[14] However, practically all the existing approaches require a thermal treatment at elevated temperatures to obtain a crystalline material, and this generally results in an irreversible agglomeration of the nanoparticles. Sol-gel,[15] hydrothermal,[16] and solvothermal[17] routes provide better control over the size, shape and agglomeration of nanoparticles, enabling fabrication of smaller nanoparticles down to 4–5 nm in size. Nevertheless, the reported NiO nanoparticles exhibit a broad particle size distribution, formation of intergrown or agglomerated crystals and a lack of dispersibility.

Here we report for the first time the preparation of ultrasmall, crystalline and dispersible NiO nanoparticles,

K. Fominykh, Dr. J. M. Feckl, J. Sicklinger,
Dr. M. Döblinger, Dr. S. Böcklein,
Prof. T. Bein, Prof. D. Fattakhova-Rohlfing
University of Munich (LMU) and Center
for NanoScience (CeNS)
Butenandtstrasse 5–13 (E), 81377, Munich, Germany
E-mail: bein@lmu.de; dina.fattakhova@cup.lmu.de

J. Ziegler
Institute of Materials Science
Jovanka-Bontschits-Str. 2, 64287, Darmstadt, Germany

Prof. L. Peter
Department of Chemistry
University of Bath
BA2 7AY, Bath, UK

Dr. J. Rathousky
J. Heyrovský Institute of Physical Chemistry, v.v.i.
Academy of Sciences of the Czech Republic
Dolejskova 3, 18223, Prague 8, Czech Republic

Dr. E.-W. Scheidt
Department of Physics
Augsburg University
86159, Augsburg, Germany

DOI: 10.1002/adfm.201303600

using a solvothermal reaction in *tert*-butanol. The size of the nanocrystals can be tuned from 2.5 to 5 nm, and electrochemical studies show that they are remarkably efficient electrocatalysts for electrochemical oxygen generation.

2. Results and Discussion

In order to overcome the previous limitations and to obtain dispersible ultrasmall colloidal NiO nanocrystals, we have developed a solvothermal approach in *tert*-butanol that involves the direct formation of crystalline nanoparticles via a chemical reaction of the precursor with the solvent. We have previously demonstrated the suitability of this reaction pathway for the fabrication of ultrasmall dispersible nanocrystals for several titanate systems,[18] but the *tert*-butanol approach had not been explored yet for other metal oxide systems. The choice of appropriate NiO precursors is decisive for the formation of nanoparticles. Nickel(II) acetylacetonate (Ni(acac)$_2$) is the most suitable precursor for dispersible crystalline NiO nanoparticles in this reaction. Formation of NiO from Ni(acac)$_2$ in *tert*-butanol requires a reaction temperature of 200 °C and a reaction time of 12 h; no product formation was observed at lower temperatures and shorter times. (Figure S1 in Supporting Information). For reaction times longer than 16 h NiO reflections are exclusively observed in the X-ray diffraction (XRD) patterns (**Figure 1**a).

The size of the phase-pure NiO nanocrystals calculated from the line broadening in the XRD corresponds to 2.5 nm after 16 h reaction time at 200 °C. For further discussion in the text the sample labeling NP-X will be used, where X is the average particle size in nm determined from XRD. The particle size increases almost linearly from 3.3 ± 0.1 nm (NP-3.3) to 4.8 ± 0.1 nm (NP-4.8) with reaction times between 17 h and 33 h, respectively (Figure 1a,b). Dried NiO nanoparticles are perfectly dispersible in ethanol after the addition of very small amounts of acetic acid. Dynamic light scattering (DLS) measurements of these transparent colloidal dispersions reveal narrow size distributions centered at 2.5 nm (NP-2.5), 3.3 nm (NP-3.3) and 4.7 nm (NP-4.8), respectively (Figure 1c). The particle size in DLS agrees well with the particle size calculated from the XRD patterns and determined from TEM images (see below). The dispersions proved to be stable, as DLS measurements showed the same particle size distribution after several weeks.

Transmission electron microscopy (TEM) images of the NiO nanoparticles NP-3.3 show non-agglomerated, defined particles with a narrow particle size distribution (**Figure 2**a, b). The lattice fringe distances (Figure 2b) in high resolution TEM images and the electron diffraction patterns (Figure 2c) are in agreement with the cubic rock salt structure of NiO deduced from XRD patterns. The average particle size obtained from the TEM images, measured and calculated over 30 particles, is 3.3 nm which is also in good agreement with the size calculated from the XRD pattern (3.3 nm, NP-3.3). When more concentrated dispersions of NiO nanoparticles were used for TEM sample preparation, we observed the formation of hexagonal supercrystals assembled from nanoparticles (Figure S2 in Supporting information). The presence of such supercrystalline assemblies is indicative for the monodisperse shape and size of the nanoparticles.[19]

Raman spectra of the as-prepared dry NiO powders (NP-3.3) show the presence of aliphatic organic groups corresponding to *tert*-BuOH solvent residues, which practically vanish after heating the samples to 100 °C. The Raman spectra of NiO powders heated to 100–240 °C show only one broad phonon vibration peak at 500–600 cm^{-1} typical for NiO[20] and similar to the spectrum of commercial NiO nanopowder (Figure S3 in Supporting Information). Heating up to 300 °C does not influence the size of the NiO nanoparticles; they only start to grow at temperatures above 350 °C (Figure S3b in Supporting Information).

Figure 3 shows the UV-visible spectra of nickel oxide nanocrystals of various sizes dispersed in ethanol with the same concentration for each sample. The distinct absorption peak around 375 nm in the UV region, as well as the weaker absorption features around 425 and 480 nm are attributed to d-d transitions of Ni(III).[21] It can be seen that smaller particles with a higher ratio of surface atoms show a stronger absorption in this region, which results in a stronger brown coloration of the dispersions (see inset in Figure 3a). This suggests that the absorption arises from Ni(III) states at the surface of the nanoparticles that

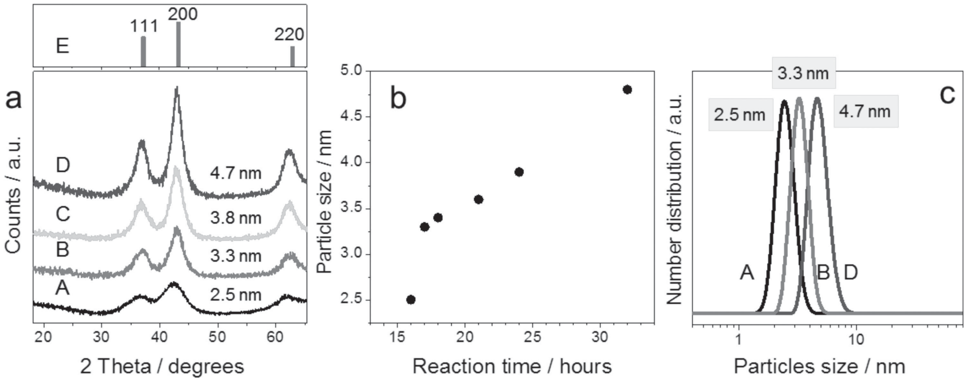

Figure 1. Characterization of NiO nanoparticles prepared from the reaction of Ni(acac)$_2$ in *tert*-BuOH at 200 °C after different reaction times: 16 h (A; sample code for further discussion in the text: NP-2.5), 17 h (B; NP-3.3), 24 h (C; NP-3.8) and 33 h (D, NP-4.8): (a) Powder XRD patterns of the dried NiO nanoparticles (E corresponds to the ICDD card number 01–071–1179, referring to NiO with rock salt structure), (b) crystalline domain size after different reaction times calculated from the XRD patterns for the most intensive NiO signal at $2\theta = 43°$ using the Scherrer equation, (c) dynamic light scattering (DLS) analysis of ethanolic dispersions of NiO nanoparticles (sample codes see above).

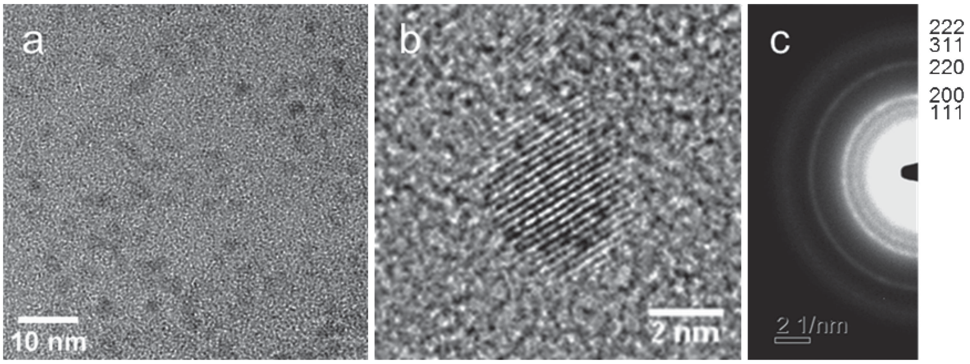

Figure 2. TEM images of the NiO nanoparticles NP-3.3: a) overview of the nanoparticles dispersed on the TEM grid; b) HRTEM image of a single NiO nanoparticle. c) Electron diffraction pattern of the NiO nanoparticles. The corresponding d-values are 2.4 (111), 2.08 (200), 1.47 (220) 1.26 (311) and 1.2 Å (222), respectively.

are probably present in the form of NiOOH or Ni(III) oxide moieties.[22] The steep absorption in the UV region below 350 nm is attributed to the band gap absorption in NiO.[23] The so-called Tauc plot in Figure S4b (Supporting information) shows a linear relation in the energy range around 3.8 to 4.1 eV for n = 2 (see UV-Vis characterization in the experimental part), indicating a direct transition as often reported for the semiconducting NiO nanoparticles.[24] This is supported by the observation that the absorption coefficients of the NiO nanoparticle dispersions in this region are in the range of 10^4–10^5 cm^{-1}, also indicating a direct transition (Figure S4a in Supporting Information). Extrapolation of the linear portion of the high energy part of the plots yields bandgap values of 3.73, 3.78 and 3.79 eV for NP-3.3, NP-3.8 and NP-4.8, respectively (Figure S4b in Supporting Information).

The attribution of the long wavelength absorption to nickel(III) states on the surface of the NiO particles is supported by magnetic measurements and by XPS analysis. The magnetic susceptibility measurements (Figure S5 in the Supporting Information) indicate an effective moment of μ_{eff} = 3.01 μ_B in the temperature region between 150 K and 250 K which is in line with the Ni(II) states with respect to a g-factor of g = 2.14. Additionally, a fit above 300 K agrees well with the presence of Ni(III) states with μ_{eff} = 3.89 μ_B and a paramagnetic Curie temperature of θ_p = 230 K. XPS measurements on the as-prepared particles (Figure 3b) revealed a binding energy for the Ni $2p_{3/2}$- and its shake up-signal of –856.5 and –862.7 eV, respectively. According to literature this can be interpreted as a nickel(III) state,[25] which could be in the form of Ni_2O_3, NiOOH or *tert*-butoxide groups attached to the surface of NiO. Quantification of the elements in XPS shows a ratio of Ni to O atoms of nearly 1:2, which could indicate that the Ni(III) states are present in the form of NiOOH on the surface of the nanoparticles (Table S1 in Supporting Information). However, this is only tentative since the surface may be contaminated. On the other hand, XPS measurements made after sputtering the surface with argon ions (Figure 3c) show a different binding energy for the Ni $2p_{3/2}$- and its shake up-signal (–854.5 and –860.9 eV), which is typical for NiO.[26] Quantification gives an atomic ratio of 1:1 confirming NiO. This is also in good agreement with the non-surface selective XRD measurements which only show a signal for NiO. In conclusion, the combination of the results of XRD, XPS, UV-Vis absorption and magnetic susceptibility measurements indicates that the as-synthesized nanoparticles have a core of NiO and some form of nickel(III) states on their surface.

The presence of Ni(III) states on the surface of the nanoparticles under ambient conditions suggests that the surface Ni atoms are highly reactive (Ni(III) states are commonly associated with the electrocatalytic activity of nickel compounds).[27,28] Therefore, we have tested our NiO nanoparticles as catalysts for the electrochemical oxidation of water. For that purpose,

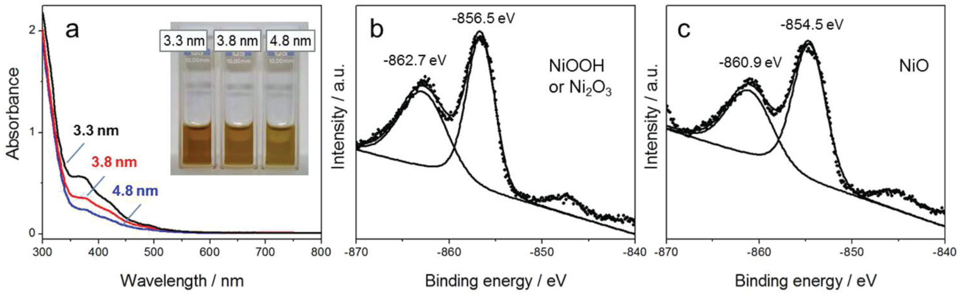

Figure 3. (a) UV-Vis absorption spectra of dispersions of NiO nanoparticles in ethanol with sizes of 3.3 nm (black, NP-3.3), 3.8 nm (red, NP-3.8) and 4.8 nm (blue, NP-4.8), and the photographs of the corresponding dispersions in an inset (5 mM concentration). X-ray photoelectron spectra (XPS) of as prepared (b) and argon polished (c) NiO nanoparticles (NP-3.3). The XPS spectra show the energy region between 840 and 870 eV corresponding to the Ni $2p_{3/2}$- and its shake up-signal. The points correspond to the experimental spectra, and the lines are the fitted curves using a Doniach Sunjic functional.

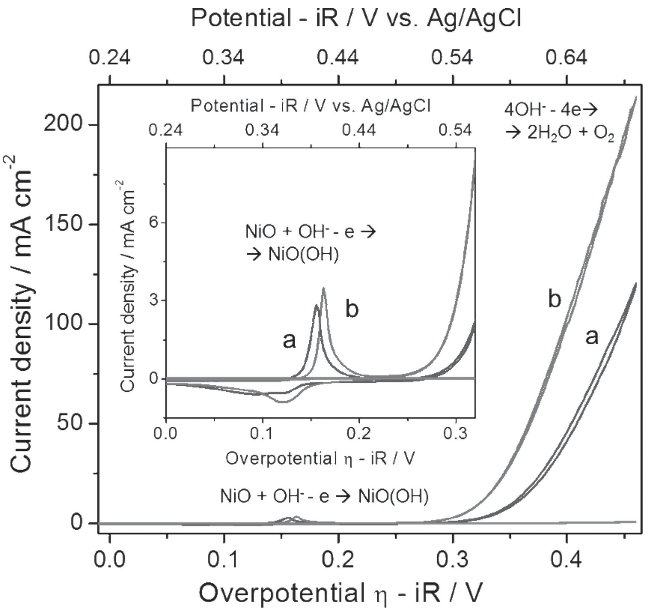

Figure 4. Cyclic voltammograms of NiO nanoparticles (NP-3.3) on Au-coated QCM electrodes in 0.5 M KOH: pre-conditioned by cycling 30 times from 0.1 to 0.7 V vs. sat. Ag/AgCl electrode with a scan rate ν = 20 mV s^{-1} (a), and electrochemically aged by applying a constant current of 7.5 mA cm^{-2} for 2.5 h (b). The gray line corresponds to a voltammogram taken on the bare Au electrode aged at the same conditions as (b). The voltammograms were taken at a scan rate of 20 mV s^{-1}.

NiO nanoparticles NP-3.3 were deposited as thin films on Au-coated QCM crystals. The use of QCM crystals enables an accurate determination of the NiO mass loading, which was 20 ± 0.8 µg cm^{-2} for the thinnest films.

Cyclic voltammograms (CVs) taken in 0.5 M KOH show the typical behavior for NiO in basic media. The CVs feature a pair of anodic and cathodic peaks centered around 0.370 V vs. Ag/AgCl corresponding to the oxidation of NiO ($NiO + OH^- - 1e^- \rightarrow NiOOH$), followed by a current due to O_2 evolution (**Figure 4**). It should be noted that only a very low current was measured on the bare Au electrode under the same conditions (see grey line in Figure 4). The current for the NiO-modified electrodes increases during the first few cycles and reaches a stable value after 30 scans, after which it remains stable and does not change anymore with prolonged cycling. Electrodes pre-conditioned in this way show a narrow anodic and a broad cathodic peak in the reversed scan, corresponding to the NiO/NiOOH redox reaction of NiO. The charge obtained from the integration of the cathodic peak corresponds to about 2.7 mC cm^{-2}, which corresponds to 10 ± 2% of the deposited NiO, independent of the mass loading on the electrode. The same fraction of electrochemically active Ni atoms was obtained for electrodes with about 2.5-times (6.0 mC cm^{-2}) and about 4.5-times (9.9 mC cm^{-2}) higher mass loadings. The measured charge closely agrees with the theoretical value corresponding to oxidation/reduction of the particle surface, which can be calculated assuming that only surface Ni atoms are electrochemically active. Using the specific surface area of the NP-3.3 NiO nanoparticles of 210 m^2 g^{-1} determined by Kr sorption (Figure S5 in Supporting Information), the real surface area (roughness factor) of the electrodes with a mass loading of 20 µg cm^{-2} is equal to 42 cm^2 cm^{-2}. This leads to a surface charge value of 2.76 mC cm^{-2} using the estimated surface density of Ni atoms of $4.08 \cdot 10^{14}$ cm^{-2} for a 110 plane. This good agreement with the electrochemically obtained charge (2.7 mC cm^{-2}) indicates that indeed surface Ni atoms are preferentially electrochemically active and that the surface of the NiO nanoparticles is also electrochemically accessible for the thicker films.

Unlike the previously reported ultrathin NiO films that completely transform to layered $Ni(OH)_2$ after prolonged electrochemical treatment,[27] the NiO electrodes assembled from our nanoparticles obtained by the *tert*-butanol route retain their integrity. The amount of Ni atoms involved in the Ni(II)/Ni(III) reaction remains practically unchanged after prolonged cycling, as determined from the charge obtained by integration of the corresponding peaks. The integrated charge remains almost constant even after extended electrochemical aging of the electrodes, which was performed galvanostatically by applying a current of 7.5 mA cm^{-2} for 2.5 h. However, the aging leads to a small shift of the NiO redox potential to more positive values (from 0.370 ± 0.001 V to 0.385 ± 0.002 V vs. Ag/AgCl, respectively). The positive shift in the redox potential is usually assigned to a phase transformation of the OH-terminated Ni atoms in basic media, from a disordered α-modification to a more ordered and more catalytically active β-modification.[27] The shift in the peak in our case is accompanied by a significant decrease in the overpotential of the OER process. The overpotential required for 1 mA cm^{-2} OER current density changes from 305 mV for the conditioned electrode to 280 mV for the aged electrode, respectively. Pre-conditioned and aged electrodes show similar Tafel slopes for the OER process of 40 mV dec^{-1} at an overpotential of 300 mV, which is consistent with the values reported for NiO[28,29] (Figure S6 in Supporting Information).

The electrodes prepared from our NiO nanoparticles show high turnover frequencies (TOF, defined as the number of O_2 molecules formed per active metal site per second) at relatively low overpotentials. The TOF calculated per active Ni atom (determined from the real surface area of the electrodes) for the aged electrodes described above is 0.29 s^{-1} at an overpotential of η = 300 mV. This value is 30 times higher than the TOF value of 0.009 s^{-1} at the same overpotential reported for IrO_x thin film electrodes that are known as some of the most active OER catalysts. The TOF value for our ultrasmall NiO particles is also significantly higher than that of 0.21 s^{-1} for Fe-doped ultrathin NiO layers, which was the highest reported value so far.[29] This makes our NiO nanoparticles very promising catalysts for electrochemical water splitting.

The dispersibility of the crystalline NiO nanoparticles allows controlled deposition of crystalline NiO layers on various flat and porous substrates. Crystalline layers with tunable thickness can therefore be processed easily from the colloidal dispersions, and importantly the films do not require further temperature treatment for crystallization. This makes it possible to deposit NiO layers on temperature-sensitive polymers or other organic materials.[12] We demonstrate the possibility of the deposition of a compact 7 nm thick NiO layer on top of a P3HT polymer layer (**Figure 5**a), which would be particularly interesting for the fabrication of organic or hybrid solar cells.[12] Furthermore,

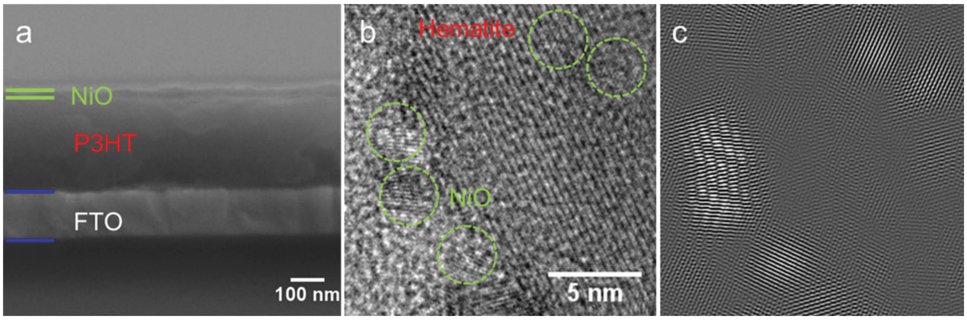

Figure 5. Deposition of NiO nanoparticles from ethanolic dispersions on different substrates: (a) as thin compact films on the top of a P3HT polymer layer (SEM image, cross-section), and as single non-agglomerated nanoparticles on crystalline mesoporous Fe_2O_3 hematite: top-view HR-TEM image (b) and its inverse FFT image (c), after masking the hematite lattice plane contribution.

the high dispersibility and the very small size of the nickel oxide nanoparticles allow us to distribute them homogeneously not only on flat substrates but also on high surface area porous host materials for possible catalytic applications. This is demonstrated in Figure 5b and c showing the homogeneous distribution of the individual non-agglomerated NiO nanoparticles on a mesoporous hematite host, which is an interesting material for photoelectrochemical water splitting.

3. Conclusion

We describe for the first time the preparation of ultrasmall, crystalline and dispersible NiO nanoparticles, which are promising candidates as catalysts for electrochemical oxygen generation. Using a solvothermal reaction in *tert*-butanol, very small nickel oxide nanocrystals can be prepared with sizes tunable from 2.5 to 5 nm and a narrow particle size distribution. The crystals are perfectly dispersible in ethanol even after drying, giving stable transparent colloidal dispersions. The nanoparticles dried at room temperature contain about 50% of organics, which can be completely removed at about 100 °C leaving an organics-free surface. Besides the decreasing particle dimensions and the increasing surface area, the nanoscaling in our synthesis leads to a changed stoichiometry of the surface compared to the bulk. Our data demonstrate that although the crystalline structure of the obtained nanocrystals corresponds to a phase-pure stoichiometric nickel(II) oxide, the decrease in the particle size evidently leads to the change in surface properties and an increased amount of electrocatalytically active sites. The nanoparticles of 3.3 nm in size demonstrate very high turn-over frequencies of 0.29 s^{-1} at an overpotential of $\eta = 300$ mV for electrochemical oxygen generation, even outperforming expensive iridium oxide catalysts. Additionally, their unique features such as the high crystallinity and dispersibility allow for the deposition of crystalline NiO layers on temperature sensitive substrates such as polymers, without the necessity of a subsequent heat treatment for crystallization. This would enable the preparation of hybrid organic/inorganic devices such as polymer solar cells. We believe that the unique features of these NiO nanocrystals provide great potential for the preparation of numerous composite materials with applications in fields such as (photo)electrochemical water splitting.

4. Experimental Section

Synthesis of NiO Nanoparticles: Nickel(II) acetylacetonate was purchased from Alfa Aesar (95 % purity). Nickel(II) acetate tetrahydrate was purchased from Aldrich (98 % purity), *tert*-butanol was purchased from Sigma-Aldrich (puriss. p.a., ACS reagent, ≥99.7%). All chemicals were used as received. *tert*-Butanol was dried over a 4 Å molecular sieve at 28 °C and filtered prior to use.

For the synthesis of nickel oxide nanoparticles with different sizes, 0.13 g (0.50 mmol) of nickel(II) acetylacetonate ($Ni(acac)_2$) was added to 14 mL of *tert*-butanol (0.147 mol) at ambient conditions forming a turbid light green suspension. The reaction mixture was stirred for 10 min, then transferred into a Teflon autoclave liner and subsequently hermetically sealed. The autoclaves were kept at 200 °C in a laboratory oven for different reaction times. The as-prepared powders were dried in air at 60 °C in a laboratory oven. The reproducibility of the reaction is very sensitive to the mass transfer conditions in the autoclave reactors, which are strongly influenced by the geometry of the autoclave and the stirring conditions. The most reproducible results were achieved for 20 mL cylindrical autoclaves (5.3 cm × 8 cm) that were rotated in the oven with a rate of ca. 250 rpm. For these conditions, about 2.5 nm (NP-2.5), 3.3 nm (NP-3.3), 3.8 nm (NP-3.8) and 4.8 nm (NP-4.8) phase-pure NiO nanoparticles were obtained after 16 h, 17 h, 24 h and 33 h reaction time, respectively. For bigger autoclaves, the reaction temperature has to be increased to 210 °C and the reaction time prolonged to at least 20 h to observe the formation of the nanoparticles.

Dispersions of the NiO nanoparticles were prepared in ethanol by the addition of concentrated acetic acid. In a typical procedure, 2.4 mg of the dried NiO powder was covered with 4 µL of acetic acid and afterwards dispersed in 1 mL of ethanol to obtain a colloidal dispersion with a NiO concentration of 0.03 mol L^{-1}.

The NiO nanoparticle dispersions (0.03 mol L^{-1}) were used for the fabrication of thin films by spin coating on fluorine-doped tin oxide coated glass (FTO) and on polymer layers of poly(3-hexylthiophene-2,5-diyl) (P3HT) deposited on FTO. 40 µL of the dispersion was cast onto the substrate with a size of 1.5 × 1.5 cm and spun at 2000 rpm for 30 s. With this method thin films with a thickness of approximately 7 nm are obtained.

For the deposition of the NiO nanoparticles on mesoporous hematite layers, 5 µL of the NiO dispersions were drop cast onto the hematite substrate with dimensions of 1 cm^2 and dried at room temperature.

Characterization: Wide angle X-ray diffraction analysis was carried out in reflection mode using a Bruker D8 Discover diffractometer with Ni-filtered CuKα-radiation (λ = 1.5406 Å) equipped with a LynxEye position sensitive detector. Powder XRD patterns of the samples were collected in a 2θ range from 5° to 67° with a step size of 0.05 and fixed counting time of 0.1 second per step. The size of the crystalline domains was calculated from the XRD patterns for the most intensive NiO signal at $2\theta = 43°$ using the Scherrer equation.

Dynamic light scattering measurements were performed on a MALVERN Zetasizer-Nano instrument equipped with a 4 mW He-Ne laser (633 nm) and an avalanche photodiode detector.

TEM measurements were carried out using a FEI Titan 80–300 equipped with a field emission gun operated at 300 kV. For the sample preparation a drop of a strongly diluted dispersion of a sample in ethanol was placed on a holey carbon coated copper grid and evaporated.

SEM images were obtained with a JEOL JSM-6500F scanning electron microscope equipped with a field emission gun operated at 4 kV. The films were prepared on silicon substrates and glued onto a brass sample holder with silver lacquer.

Raman spectroscopy was carried out using a LabRAM HR UV-Vis (HORIBA JOBIN YVON) Raman Microscope (OLYMPUS BX41) with a SYMPHONY CCD detection system and a He-Ne laser (λ = 633 nm). Spectra were recorded using a lens with a 100-fold magnification.

Thermogravimetric analysis of the samples was performed on a NETZSCH STA 440 C TG/DSC (heating rate of 10 K min^{-1} in a stream of synthetic air of about 25 mL min^{-1}).

X-ray photoelectron spectroscopy (XPS) analysis of the particles on a silicon substrate was performed using a VSW HA 100 electron analyzer and the Kα radiation provided by a non monochromatized magnesium anode system (Mg Kα = 1253.6 eV). Ar ion polishing was done at 1000 eV for 10 minutes. The recorded elemental peaks were fitted using a Doniach-Sunjic function[30] and the elemental ratios were calculated by the equation: $X_A/X_B = (I_A/I_B)(S_B/S_A)$, where I_A/I_B is the ratio of fitted areas, and S is the sensitivity factor.

The UV-visible spectra of the samples were measured with a Perkin Elmer Lambda 1050 spectrophotometer equipped with an integrating sphere.

The bandgap E_g of NiO was determined from the measured spectra using the relationship: $h\nu - E_g \propto (\alpha h\nu)^n$, where $h\nu$ is the photon energy, α (alpha) is the absorption coefficient, and the exponential factor n being either 2 for a direct allowed transition or ½ for an indirect allowed transition. The absorption coefficient alpha was calculated from the absorbance with the following equations: $A = -\log_{10}(I_t/I_0) = \varepsilon\, c_{\text{solid}} l$, where A is the absorbance, I_0 is the incident light, I_t is the transmitted light, ε is the molar absorption coefficient and l is the optical path length (1 cm).

$$-\ln(I_t/I_0) = \alpha l = -2.303\log_{10}(I_t/I_0)$$

$$= \varepsilon\, c_{\text{solid}} l, \quad \alpha = 2.303\varepsilon\, c_{\text{solid}}$$

The concentration c_{solid} of the solid NiO was calculated from the molar volume V_M that is given by the molar mass M_{NiO} (74.69 g mol^{-1}) and the density ρ_{NiO} (6.67 g cm^{-3}) of NiO:

$$c_{\text{solid}} = 1/V_M = \rho/\text{M} = 89.3\ \text{moldm}^{-3} = 89.3\ \text{M}$$

ε was calculated from the concentration of nickel oxide in the dispersion ($c_{\text{dispersion}}$ = 5 mM):

$$\varepsilon = A/(c_{\text{dispersion}} l) = A/5\,10^{-3},$$

$$\alpha(\lambda) = 2.303(A(\lambda)/5\,10^{-3})89.3\ \text{cm}^{-1}$$

A Magnetic Property Measurement System (MPMS) from Quantum Design was used to determine the temperature dependent dc-susceptibility $\chi(T)$ and the magnetic field dependent magnetization $m(H)$. These measurements were performed in a temperature range between 2 and 400 K and in magnetic fields up to 10 kOe. A small amount of NiO powder (9.41 mg) was mounted between two KEL-F staves fitted in a straw. The susceptibility data are normalized to one mol of the respective formula unit (f.u.).

Electrode Preparation: The electrodes were prepared by deposition of the dispersed nickel oxide nanoparticles either by spin coating or by drop casting on QCM crystals (KVG 10 MHz QCM devices with gold electrodes from Quartz Crystal Technology GmbH). In a typical drop casting procedure, 4 µL of nickel oxide dispersion was cast on the Au layer of a QCM crystal. A mask was used to cover the non-active surface of the QCM chip exposing an area of 0.196 cm^2. The loaded QCM crystal was dried in air at ambient conditions for 5 min. For the spin coating method 8 µL of nickel oxide dispersion was deposited on a masked QCM crystal and spun at 1000 rpm for 10 s. The QCM electrodes prepared with both methods were subsequently heated to 240 °C in a laboratory oven with a heating ramp of 4 °C min^{-1} and a dwell time of 2 h.

Electrochemical Measurements: Electrochemical measurements were performed in a three-electrode setup using an Autolab potentiostat/galvanostat PGSTAT302N with FRA32M module operating with Nova 1.9 software. All the measurements were performed in 0.5 M KOH electrolyte solution (Sigma-Aldrich, volumetric solution) at pH 13.43. Pt mesh (2 cm^2) was used as a counter electrode. Au/QCM crystals with NiO nanoparticles deposited on one side (preparation is described above) were used as working electrodes. To provide an electric connection to the QCM electrode, a silver wire was connected to the respective part of the QCM crystals using silver lacquer. The silver lacquer and the wire were sealed afterwards in inert two-component epoxy resin (Gatan, Inc). All potentials were measured vs. Ag/AgCl/KCl sat. reference electrode, whose potential is +0.989 V vs. the reversible hydrogen electrode (RHE) at pH 13.43 (+0.197 V vs. NHE). The electrochemical data were corrected for uncompensated resistance R_s. The R_s was determined as minimum total impedance in the frequency regime between 10 and 50 kHz at open circuit conditions and at a potential of 0.2 V vs. Ag/AgCl electrode, where no Faradaic processes take place. The resistance was taken as an average of 3 measurements, 90% of this value was compensated. R_s was typically around 6–7 Ohm for the NiO-coated Au/QCM electrodes. The overpotential η was calculated using the equation $\eta = E - E_{OER} - iR_s$, where E is the potential recorded vs. Ag/AgCl reference electrode, E_{OER} is the reversible potential of the OER vs. Ag/AgCl reference electrode (0.240 V at pH 13.43), and i is the current. Current densities are calculated using the geometric surface area of the Au/QCM electrode (0.196 cm^2).

The pre-conditioning of the NiO electrodes was achieved using cyclic voltammetry (CVA). The electrodes were cycled between 0 V and 0.7 V vs. Ag/AgCl in 0.5 M KOH at a scan rate of 20 mV s^{-1} until the current had reached stable values and did not change anymore with repetitive cycling (typically 30 cycles). The CVA measurements on these pre-conditioned electrodes were made at scan rates from 2 mV s^{-1} to 20 mV s^{-1} without stirring the electrolyte. The aging was performed galvanostatically by applying a current density of 7.5 mA cm^{-2} for 2.5 h in a two-electrode mode in a stirred 0.5 M KOH solution. The electrolyte was replaced after the aging procedure by a fresh one for subsequent CVA measurements.

The turn-over frequency (TOF) at an overpotential of η = 0.3 V was calculated on the basis of surface Ni atoms according to: $\text{TOF} = j/(4\cdot F\cdot n_{\text{surf}})$, where j is the current density (A cm^{-2}), F is Faraday's constant, and n_{surf} is the surface concentration of Ni atoms (mol cm^{-2}). The surface concentration of Ni atoms was calculated from the mass loading of the films m (g cm^{-2}), the BET surface area of the nanoparticles of $2.1\cdot 10^6$ cm^2 g^{-1} determined with Kr sorption and estimated surface density N_{NiO} of Ni atoms in NiO of $4.08\cdot 10^{14}$ cm^{-2} according to: $n_{\text{surf}} = m\cdot \text{BET}\cdot N_{\text{NiO}}/N_A$, where N_A is the Avogadro constant.

Alternatively, the number of electrochemically accessible Ni atoms was determined from the charge corresponding to the NiO redox reaction according to the equation: $\text{NiO} + \text{OH}^- - 1e^- \rightarrow \text{NiOOH}$. As the charge obtained from the anodic peak of the NiO redox process may contain some contribution from the OER process we have used the cathodic peak to determine the amount of the catalytically active Ni atoms.

Supporting Information

Supporting Information is available from the Wiley Online Library or from the author.

Acknowledgements

K. Fominykh and J. M. Feckl contributed equally to this work. Financial support from the DFG (SPP 1613), the NIM cluster (DFG), the research network 'Solar Technologies Go Hybrid' (State of Bavaria), the Center for NanoScience (CeNS), and LMUmentoring is gratefully acknowledged.

Received: October 22, 2013
Revised: November 27, 2013

[1] a) H. Kuhlenbeck, S. Shaikhutdinov, H.-J. Freund, *Chem. Rev.* **2013**, *113*, 3986; b) T. W. Kim, S. J. Hwang, S. H. Jhung, J. S. Chang, H. Park, W. Choi, J. H. Choy, *Adv. Mat.* **2008**, *20*, 539.

[2] a) P. Poizot, S. Laruelle, S. Grugeon, L. Dupont, J. M. Tarascon, *Nature* **2000**, *407*, 496; b) H. Liu, G. Wang, J. Liu, S. Qiao, H. Ahn, *J. Mater. Chem.* **2011**, *21*, 3046.

[3] a) Q. Lu, M. W. Lattanzi, Y. Chen, X. Kou, W. Li, X. Fan, K. M. Unruh, J. G. Chen, J. Q. Xiao, *Angew. Chem. Int. Ed.* **2011**, *50*, 6847; b) S. I. Kim, J. S. Lee, H. J. Ahn, H. K. Song, J. H. Jang, *ACS Appl. Mater. Interf.* **2013**, *5*, 1596.

[4] D. T. Gillaspie, R. C. Tenent, A. C. Dillon, *J. Mater. Chem.* **2010**, *20*, 9585.

[5] N. D. Hoa, S. A. El-Safty, *Chem. Eur. J.* **2011**, *17*, 12896.

[6] B. Zhao, X.-K. Ke, J.-H. Bao, C.-L. Wang, L. Dong, Y.-W. Chen, H.-L. Chen, *J. Phys. Chem. C* **2009**, *113*, 14440.

[7] X. Cao, Y. J. Xu, N. Wang, *Sens. Actuat. B* **2011**, *153*, 434.

[8] M.-M. Titirici, M. Antonietti, A. Thomas, *Chem. Mater.* **2006**, *18*, 3808.

[9] R. K. Joshi, J. J. Schneider, *Chem. Soc. Rev.* **2012**, *41*, 5285.

[10] H. Pang, Q. Lu, Y. Li, F. Gao, *Chem. Commun.* **2009**, 7542.

[11] Y. F. Yuan, X. H. Xia, J. B. Wu, J. L. Yang, Y. B. Chen, S. Y. Guo, *Electrochem. Comm.* **2010**, *12*, 890.

[12] J. R. Manders, S.-W. Tsang, M. J. Hartel, T.-H. Lai, S. Chen, C. M. Amb, J. R. Reynolds, F. So, *Adv. Funct. Mater.* **2013**, *23*, 2993.

[13] M. Niederberger, N. Pinna, Metal Oxide Nanoparticles in Organic Solvents, Springer, Dordrecht **2009**.

[14] a) H. G. Zhang, X. D. Yu, P. V. Braun, *Nat. Nanotechnol.* **2011**, *6*, 277; b) A. K. Mishra, S. Bandyopadhyay, D. Das, *Mater. Res. Bull.* **2012**, *47*, 2288; c) B. Xia, I. W. Lenggoro, K. Okuyama, *Chem. Mater.* **2002**, *14*, 2623; d) D. S. Wang, T. Xie, Q. Peng, S. Y. Zhang, J. Chen, Y.D. Li, *Chem. Eur. J.* **2008**, *14*, 2507.

[15] a) S. Pilban Jahromi, N. M. Huang, M. R. Muhamad, H. N. Lim, *Ceramics Int.* **2013**, *39*, 3909; b) K. Hayat, M. A. Gondal, M. M. Khaled, S. Ahmed, *J. Molec. Catal. A* **2011**, *336*, 64.

[16] K. Sue, S.-i. Kawasaki, M. Suzuki, Y. Hakuta, H. Hayashi, K. Arai, Y. Takebayashi, S. Yoda, T. Furuya, *Chem. Eng. J.* **2011**, *166*, 947.

[17] E. R. Beach, K. Shqau, S. E. Brown, S. J. Rozeveld, P. A. Morris, *Mater. Chem. Phys.* **2009**, *115*, 371.

[18] a) J. M. Feckl, K. Fominykh, M. Doblinger, D. Fattakhova-Rohlfing, T. Bein, *Angew. Chem. Int. Ed.* **2012**, *51*, 7459; b) J. M. Szeifert, J. M. Feckl, D. Fattakhova-Rohlfing, Y. J. Liu, V. Kalousek, J. Rathousky, T. Bein, *J. Amer. Chem. Soc.* **2010**, *132*, 12605; c) Y. J. Liu, J. M. Szeifert, J. M. Feckl, B. Mandlmeier, J. Rathousky, O. Hayden, D. Fattakhova-Rohlfing, T. Bein, *ACS Nano* **2010**, *4*, 5373.

[19] C. Desvaux, C. Amiens, P. Fejes, P. Renaud, M. Respaud, P. Lecante, E. Snoeck, B. Chaudret, *Nat. Mater.* **2005**, *4*, 750.

[20] N. Mironova-Ulmane, A. Kuzmin, I. Steins, J. Grabis, I. Sildos, M. Pars, Funct. Mater. Nanotechnol., Vol. *93* (Eds: A. Sternberg, I. Muzikante), IOP Publishing Ltd, Bristol **2007**.

[21] A. Gorschluter, H. Merz, *Phys. Rev. B* **1994**, *49*, 17293.

[22] A. R. Gonzalezelipe, J. P. Holgado, R. Alvarez, G. Munuera, *J. Phys. Chem.* **1992**, *96*, 3080.

[23] D. Adler, J. Feinleib, *Phys. Rev. B* **1970**, *2*, 3112.

[24] a) X. L. Li, X. X. Zhang, Z. R. Li, Y. T. Qian, *Solid State Commun.* **2006**, *137*, 581–584; b) F. Davar, Z. Fereshteh, M. Salavati-Niasari, *J. Alloys Comp.* **2009**, *476*, 797–801.

[25] a) M. C. Biesinger, B. P. Payne, L. W. M. Lau, A. Gerson, R. S. C. Smart, *Surf. Interface Anal.* **2009**, *41*, 324; b) B. W. Hoffer, A. D. van Langeveld, J. P. Janssens, R. L. C. Bonne, C. M. Lok, J. A. Moulijn, *J. Catal.* **2000**, *192*, 432; c) N. S. McIntyre, M. G. Cook, *Anal. Chem.* **1975**, *47*, 2208.

[26] P. Selvam, B. Viswanathan, V. Srinivasan, *J. Electron Spectrosc. Relat. Phenom.* **1989**, *49*, 203.

[27] M. E. G. Lyons, M. P. Brandon, *Int. J. Electrochem. Sci.* **2008**, *3*, 1386.

[28] B. S. Yeo, A. T. Bell, *J. Phys. Chem. C* **2012**, *116*, 8394.

[29] L. Trotochaud, J. K. Ranney, K. N. Williams, S. W. Boettcher, *J. Am. Chem. Soc.* **2012**, *134*, 17253.

[30] S. Doniach, M. Sunjic, *J. Phys. C* **1970**, *3*, 285.